CHEMISTRY
A European Journal

A Journal of
ChemPubSoc Europe

Accepted Article

Title: 1,1'-Binaphthyl Consisting of Two Donor-π-acceptor Subunits : a General Skeleton for Temperature-Dependent Dual Fluorescence

Authors: Di-Hong Liu, Zuo-Bang Sun, Zheng-Hua Zhao, Qian Peng, and Cui-Hua Zhao

To be cited as: *Chem. Eur. J.* 10.1002/chem.201901719

Link to VoR: http://dx.doi.org/10.1002/chem.201901719

Supported by
ACES

WILEY-VCH

10.1002/chem.201901719

WILEY-VCH

FULL PAPER

1,1'-Binaphthyl Consisting of Two Donor-π-acceptor Subunits：a General Skeleton for Temperature-Dependent Dual Fluorescence

Di-Hong Liu,[a] Zuo-Bang Sun,[a] Zheng-Hua Zhao,[a] Qian Peng*[b] and Cui-Hua Zhao,*[a]

Abstract: The temperature-dependent dual fluorescence with anti-Kasha's rule is a great interest but very challenging property for small organic molecules. Inspired by the highly sensitive temperature-dependent dual fluorescence of 2,2'-bis(dimethylamino)-6,6'-bis(dimesitylboryl)-1,1'-binaphthyl (**BNMe$_2$-BNaph**), which essentially consists of two D-π-A subunits, we herein have explored the importance of its structure feature and the general utility of this molecular design. It was found the reference compound **MBNMe$_2$-BNaph**, which lacks one electron-accepting Mes$_2$B, shows less sensitive temperature-dependent dual fluorescence, suggesting that the structure of **BNMe$_2$-BNaph** symmetrically consisting of two D-π-A subunits is very important to achieve highly sensitive temperature-dependent dual fluorescence. In addition, it was found another two 1,1'-binaphthyls, **CHONMe$_2$-BNaph** and **CNNMe$_2$-BNaph**, which also consist of two D-π-A subunits with Mes$_2$B groups replaced by CHO and CN, respectively, also show temperature-dependent dual fluorescence with fluorescence changing in a similar manner as **BNMe$_2$-BNaph**, denoting the general utility of the current molecular design for the temperature-dependent dual fluorescence. In addition, the temperature-dependent dual fluorescence behaviours, such as relative intensity of two emission bands, the separation of two emissions bands and the sensitivity of fluorescence intensity ratio versus temperature, are greatly influence by the electron-acceptors.

Introduction

The temperature-dependent dual fluorescence is a highly desired property for fluorescent materials owing to its great application in the temperature measurement utilizing the ratiometric fluorescence intensity method. Compared with the widely-used single fluorescence intensity method, the temperature measurement based on the change in the intensity ratio of two emission bands is less dependent on the external factors, such as background fluorescence, fluorophore concentration, and source power.[1] In addition, the ratiometric fluorescence intensity measurement can provide a high degree of visualization under UV illumination. To realize the ratiometric fluorescence measurement of temperature, the hybrid nanoparticles,[2] polymer systems,[3] and rare-earth complexes have been usually adopted.[4] These systems either require complicated fabrication processes and extra calibration of physiochemical properties between two different components or are unstable in polar solvents and show remarkable fluorescence quenching to oxygen. To overcome these disadvantages, the ratiometric fluorescence thermometers based on the single-component small organic molecules (SOMs) can provide good solutions. However, the design of such fluorophores is a very challenging issue.[5] According to Kasha's rule, the luminescence generally occurs only from the lowest singlet excited state (S_1).[6] As a consequence, the dual fluorescence is an anomalous photophysical phenomenon for SOMs.

To achieve dual fluorescence for SOMs, one strategy is to construct fluorescent molecules utilizing a nonplanar flexible skeleton, which easily undergoes conformational planarization in S_1 state to give rise to a temperature-dependent dual fluorescence corresponding to the two different geometries of S_1 state without violation of Kasha's rule. This strategy has been well demonstrated by the cyclooctatetraene[7] and dihydrodibenzo[a,c]phenazine derivatives.[8] Another more general strategy is to design π-systems with "normal" donor-π-acceptor (D-π-A) structure.[9] In addition to a localized excited (LE) state, the presence of a fluorescent intramolecular charge transfer (ICT) excited state is usually proposed to explain the dual fluorescence of these systems. The ICT state is formed via the geometric rearrangement (planarization or twisting at the bridge between donor and acceptor units) following excitation to the LE state or by direct excitation from the ground state (S_0). In the latter case, the two emissive states are structurally different and usually correspond to S_1 and the second excited state (S_2), respectively, which is virtually ascribed to the anti-Kasha behaviour. In spite of the a number of dual fluorescent SOMs with D-π-A structure, the fluorescence of these molecules is usually not sensitive to temperature due to the absence of thermal equilibrium, for which an appropriately small energy gap between two excited states is required.[10] In continuous with our research on the emissive triarylborane-based SOMs with D-π-A structure,[11] we have recently reported a triarylborane compound, 2,2'-bis(dimethylamino)-6,6'-bis(dimesitylboryl)-1,1'-binaphthyl (**BNMe$_2$-BNaph**) (Figure 1a),[12] which displays temperature-dependent dual fluorescence. The well-separation of two emission bands together with the high sensitivity of the fluorescence intensity ratio versus temperature are expected to make this compound behave as a highly sensitive ratiometric fluorescence thermometer. Very different from the "normal" D-π-A molecules, this compound essentially consists of two independent D-π-A subunits, in which dimesitylboryl (Mes$_2$B) acts as a strong electron-acceptor.[13] The investigation on the fluorescence mechanism suggested the two emission bands arise from the deactivations of S_1 and S_2 states, which are essentially ascribable to the inter-subunit and intra-subunit CT transitions, respectively. The existence of thermal equilibrium between the

[a] D.-H. Liu, Z.-B. Sun, Z.-H. Zhao, Prof. Dr. C.-H. Zhao
School of Chemistry and Chemical Engineering
Shandong University
Jinan, 250100, (P. R. China)
E-mail: chzhao@sdu.edu.cn
[b] Prof. Dr. Q. Peng
Key Laboratory of Organic Solids
Beijing National Laboratory for Molecular Science (BNLMS)
Beijing 100190 (P. R. China)
E-Maill: qpeng@iccas.ac.cn
Supporting information for this article is given via a link at the end of the document.((Please delete this text if not appropriate))

10.1002/chem.201901719

first two excited states is due to their small energy difference at the Frank-Condon geometry upon excitation from S_0 state.[12] Promoted by the fascinating photophysical properties of **BNMe$_2$-BNaph**, we were interested in the importance of its unique structure feature and the general utility of the molecular design to achieve the temperature-dependent dual fluorescence. Herein, we have designed and synthesized a reference compound, Mes$_2$B-substituted 1,1'-binaphthyl, **MBNMe$_2$-BNaph** (Figure 1b), which contains one less Mes$_2$B group, and other electron-acceptors-substituted 1,1'-binaphthyls, which are also characteristic of the composition of two D-π-A subunits with Mes$_2$B replaced by other electron-acceptors, such as formyl (CHO) (**CHONMe$_2$-BNaph**), cyano (CN) (**CNNMe$_2$-BNaph**) (Figure 1a). The photophysical properties of these compounds were fully characterized experimentally and theoretically to illustrate the effect of structure modification on the temperature-dependent dual fluorescence property.

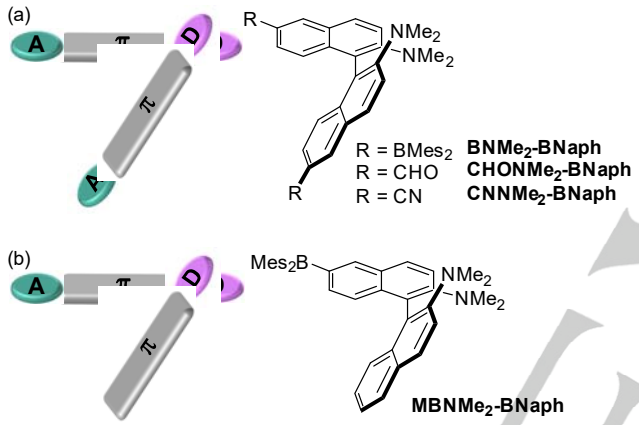

Figure 1. Schematic presentation and structures of (a) 1,1'-binaphthyls consisting of two D-π-A subunits, and (b) the related reference compound.

Results and Discussion

Synthesis

All the 1,1'-binaphthyl derivatives were prepared from a common dibromide precursor,[12] 6,6'-dibromo-2,2'-bis(N,N-dimethylamino)-1,1'-binaphthyl (**BrNMe$_2$-BNaph**), as shown in Scheme 1. To obtain **MBNMe$_2$-BNaph**, which contains only one Mes$_2$B, we first tried the dilithiation of **BrNMe$_2$-BNaph** and then quenching with one equivalent of Mes$_2$BF. This method always produced too complicated reaction mixture to get the pure product. Finally, **MBNMe$_2$-BNaph** was obtained through borylation of the corresponding monobromide precursor, which was obtained via lithiation of **BrNMe$_2$-BNaph** with one equivalent of *n*-BuLi and quenching with MeOH and used as the crude product without further purification. For the synthesis of 1,1'-binaphthyls consisting of two D-π-A subunits, only the transformation of bromo to the corresponding electron-acceptors is required. The transformation of bromo to CHO was accomplished by the complete lithiation of **BrNMe$_2$-BNaph** followed by electronic quenching with dimethylformamide (DMF). To realize the transformation of bromo to CN, the Ullman coupling reaction of **BrNMe$_2$-BNaph** with CuCN was utilized.[14] All the newly prepared 1,1'-binaphthyl derivatives were full characterized by ^{1}H NMR, ^{13}C NMR and high-resolution mass (HRMS).

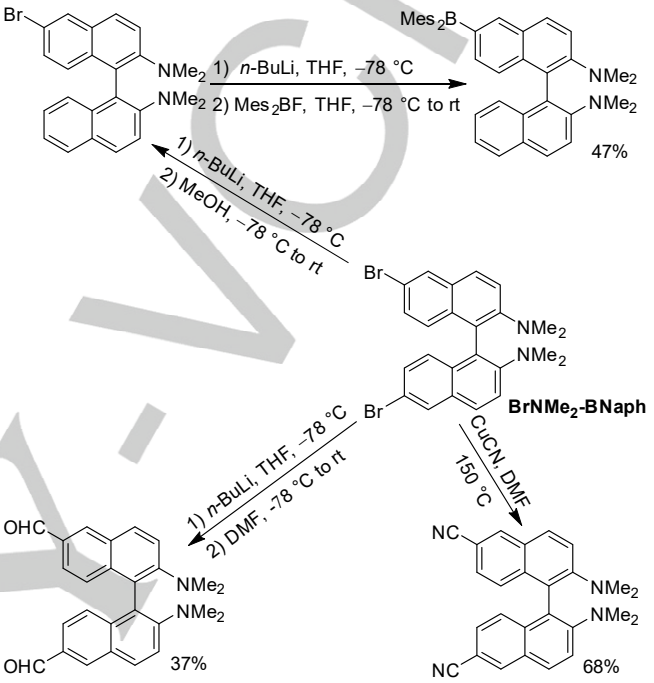

Scheme 1. Synthesis of 1,1'-binaphthyls consisting of two D-π-A subunits and the related reference compound.

Photophysical properties of MBNMe$_2$-BNaph

With regard to the photophysical property, the most important feature for **BNMe$_2$-BNaph** is the highly sensitive temperature-dependent dual fluorescence with well-separation of two emission bands (Figure S1).[12] To explore the importance of the unique structure feature of **BNMe$_2$-BNaph** for the temperature-dependent dual fluorescence, the photophysical properties of the reference compound, **MBNMe$_2$-BNaph**, were first fully characterized for a detailed comparison. Compared with **BNMe$_2$-BNaph**, the 1,1'-binaphthyl **MBNMe$_2$-BNaph** lacks one electron-accepting Mes$_2$B group. It was found this minor structure change resulted in remarkable difference in their photophysical properties. Figure 2a shows the absorption and fluorescence spectra of both compounds in MOE. In the absorption, although the longest maxima are located at the same positions (Table S1), the absorption intensity of **MBNMe$_2$-BNaph** is lower relative to **BNMe$_2$-BNaph** (log ε = 4.27 for **MBNMe$_2$-BNaph**; 4.32 for **BNMe$_2$-BNaph**). Regarding the fluorescence, it is interesting to find that **MBNMe$_2$-BNaph** also exhibits dual fluorescence. In addition to the main band at 473 nm, a shoulder emission band was observed at the longer wavelength (ca. 535). It was noted

10.1002/chem.201901719

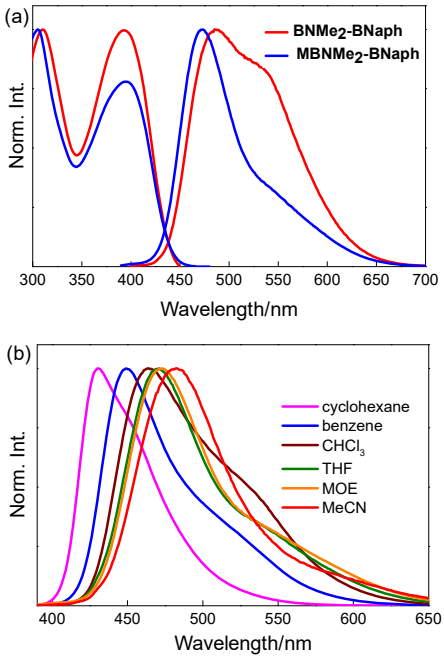

Figure 2. (a) Absorption and fluorescence spectra of **MBNMe$_2$-BNaph** and **BNMes$_2$-BNaph** in MOE, and (b) fluorescence spectra of **MBNMes$_2$-BNaph** in various solvents.

that the shorter wavelength band is much stronger than the longer shoulder band with an intensity ratio of 2.8, which is in contrast to the very close intensity of two emission bands in **BNMe$_2$-BNaph**. The intensity ratio of two emission bands in **BNMe$_2$-BNaph** is only 1.2. With the increasing solvent polarity, **MBNMe$_2$-BNaph** shows great positive solvotachromism for both emission bands (Figure 2b). A comparison of fluorescence in various solvents suggests the shorter wavelength band of **MBNMe$_2$-BNaph** is slightly shorter ($\Delta\lambda$ = 7–13 nm) than **BNMe$_2$-BNaph**. However, the longer wavelength band of **MBNMe$_2$-BNaph** is always very weak and coalesced with the tail of the shorter emission band in various solvent, which makes it difficult to determine its exact position. To further understand the longer emission property of **MBNMe$_2$-BNaph**, its fluorescence spectra in various solvents were further characterized at –20 °C, at which the longer wavelength band becomes much stronger (Figure S3, Table S3). Similar to **BNMe$_2$-BNaph**, the solvatochromism of the longer wavelength band of **MBNMe$_2$-BNaph** is more significant than the shorter wavelength band. From benzene to acetonitrile, the longer wavelength band exhibits a red shift of 60 nm from 510 nm to 570 nm while the shorter wavelength band is only shifted by 34 nm from 451 nm to 485 nm. In addition, the position of the longer wavelength band in **MBNMe$_2$-BNaph** is not very different with that of **BNMe$_2$-BNaph** ($\Delta\lambda$ = 5–8 nm). The preliminary results on the photophysical properties of **MBNMe$_2$-BNaph** suggest the abstraction of one electron-accepting Mes$_2$B from **BNMe$_2$-BNaph** mainly has great influence on the intensity ratio of two emission bands.

Considering the dual fluorescence of **MBNMe$_2$-BNaph**, it is of great interest to examine the temperature influence on its

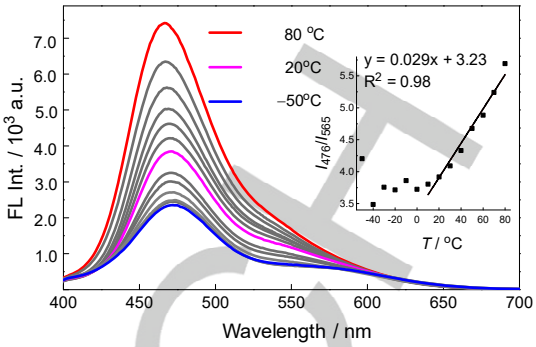

Figure 3. Fluorescence spectra of **MBNMe$_2$-BNaph** at various temperatures (1.0×10^{-5} M in MOE). Inset: fluorescence ratios between shorter and longer wavelength bands versus temperature.

photophysical properties. As shown in Figure 3, the fluorescence of **MBNMe$_2$-BNaph** is also sensitive to temperature. Within the examined temperature range from –50 to 80 °C, the fluorescence continuously becomes stronger as the temperature increases. In addition, the intensity of the shorter emission band increases more rapidly. Consequently, the fluorescence intensity ratio between shorter and longer wavelength bands increases as a whole. These features are similar to **BNMe$_2$-BNaph**. Regarding the temperature-dependent fluorescence property, the following different characteristics are also noted between **MBNMe$_2$-BNaph** and **BNMe$_2$-BNaph**. The fluorescence of **MBNMe$_2$-BNaph** is always predominantly dominated by the shorter wavelength band, even at –50 °C, which is accompanied by the little change of fluorescence colour (Figure S4a). In contrast, the longer wavelength band turns stronger than the shorter wavelength band when the temperature is lower than 0 °C for **BNMe$_2$-BNaph**. Consistent with this phenomenon, the fluorescence intensity ratio between the shorter and longer wavelength bands of **MBNMe$_2$-BNaph** increases less rapidly with increasing temperature, as evidenced by a smaller slope (0.029). Consequently, the fluorescence of **MBNMe$_2$-BNaph** is less sensitive to temperature. Moreover, the fluorescence intensity ratio of **MBNMe$_2$-BNaph** increases linearly within a much narrower temperature range. The linear relationship between the fluorescence intensity ratio and temperature was observed from 10 to 80 °C for **MBNMe$_2$-BNaph**. Despite the remarkable fluorescence changes, little changes were observed in the absorption of **MBNMe$_2$-BNaph** (Figure S4b). With the increasing –temperature, the longest maximum is gradually shifted from 400 nm –50 °C to 390 nm at 80 °C with the slight decrease of absorption intensity, which is in the same trend as **BNMe$_2$-BNaph**. Judging from the sensitivity and temperature range for linear relationship between fluorescence intensity ratio and temperature, **BNMe$_2$-BNaph** is a more ideal candidate for the ratiometric fluorescence thermometer.

For **BNMe$_2$-BNaph**, its dual fluorescence property has been reasonably explained by the deactivation of two different excited states (S_1 and S_2) with anti-kasha's rule (Figure S7 and S8).[12] In S_0 state, its lowest occupied molecular orbital (LUMO) and LUMO+1 are almost degenerate in energy with electron distributed over the dimesitylborylnaphthyl group of one subunit.

10.1002/chem.201901719

As a consequence, the S_1 and S_2 excitations show very small differences in energy (ΔE = 0.07 eV) because their transitions are essentially assignable to the transitions from HOMO localized on the entire 2,2'-diamino-1,1'-binaphthyl skeleton to LUMO and LUMO+1, respectively. In addition, the transitions to the first two excited two states show close oscillator strengths (0.1213 and 0.1331), suggesting their similar absorption properties. The deactivation of S_1 is essentially an inter-subunit CT from the HOMO on the dimethylaminonaphthyl group of one subunit to the LUMO on the dimesitylborylnaphthyl moiety of another subunit while the deactivation of S_2 is mainly dominated by an intra-subunit CT from the dimethylamino moiety to the dimesitylboryl group of the same subunit. More importantly, the oscillator strength of S_2 deactivation (0.2627) is about 90 times of that of S_1 state (0.0029).[12] Here, the temperature dependence of dual fluorescence can be explained by the close energy between S_1 and S_2 at the Frank-Condon geometry, which would enable a possible thermal equilibrium population between them.[10b] And the much larger oscillator strength of S_2 state deactivation than that of S_1 can give a good explanation for the significantly enhanced fluorescence intensity and rapidly increased fluorescence intensity ratio between shorter and longer wavelength bands with increasing temperature.

To elucidate the underlying origin for the different temperature-dependent dual fluorescence behaviours between **MBNMe$_2$-BNaph** and **BNMe$_2$-BNaph**, systematic calculations were carried out for **MBNMe$_2$-BNaph**. A detailed comparison of the theoretical calculation results revealed that the S_1 state of these two Mes_2B-substituted 1,1'-binaphthyls have similar electronic nature, in terms of either the electron distributions of the involved frontier orbitals or the oscillator strengths of the corresponding excitation and deactivation processes (Figure 4). However, great differences were found for the S_2 state between them. The S_2 state excitation in **MBNMe$_2$-BNaph** corresponds to a HOMO-1→LUMO transition, in which the HOMO-1 still spreads on the entire 2,2'-diamino-1,1'-binaphthyl skeleton like HOMO but with 0.28 eV lower in energy. Consequently, the energy difference between S_1 and S_2 states at the Frank-Condon geometry becomes much larger (0.25 eV) for **MBNMe$_2$-BNaph**. This larger energy gap probably implies a higher temperature to trigger the S_2 state thermal population. In addition, the oscillator strength of S_2 state excitation is about 1.7 times of the S_1 state excitation, which indicates a higher probability of excitation to S_2 state and presumably accounts in part for the domination of shorter wavelength band in the fluorescence. The S_2 state deactivation of **MBNMe$_2$-BNaph** is still dominated by an inter-subunit charge transfer, which in fact consists of the transition from HOMO localized on the dimethylaminonaphthyl of the subunit containing no Mes_2B to the LUMO+1 spreading over naphthyl of the subunit containing Mes_2B with little contribution from vacant p orbital of boron. Consistent with the electron distributions of the first two excited states, it was noted that the amino of the subunit containing no Mes_2B is conjugated more efficiently with the attached naphthylgroup than the amino of another subunit in both S_1 and S_2 states, as demonstrated by its more planarized geometry, smaller dihedral angle between NC_3 plane and naphthyl group, and as well as shorter N-C(Naphthyl) bond length (Table S5). It was also noted that the conjugation between boryl and the attached naphthyl is more efficient in S_1 state than in S_2 State, which is evidenced by the smaller dihedral angle between BC_3 and the attached naphthyl group and the shorter B-C (naphthyl) bond length. More notably, the oscillator strength of S_2 deactivation (0.014) is only 7 times of that of S_1 state. The less significant contrast of the oscillator strengths between the S_1 and S_2 deactivations in **MBNMe$_2$-BNaph** is probably one possible reason that causes lower sensitivity of fluorescence intensity ratio versus temperature. The theoretical results combined with the experiment results may suggest the superiority of **BNMe$_2$-BNaph** over **MBNMe$_2$-BNaph** in performance as the ratiometric fluorescence thermometer. Therefore, the unique symmetrical structure of **BNMe$_2$-BNaph**, which consists of two D-π-A subunits

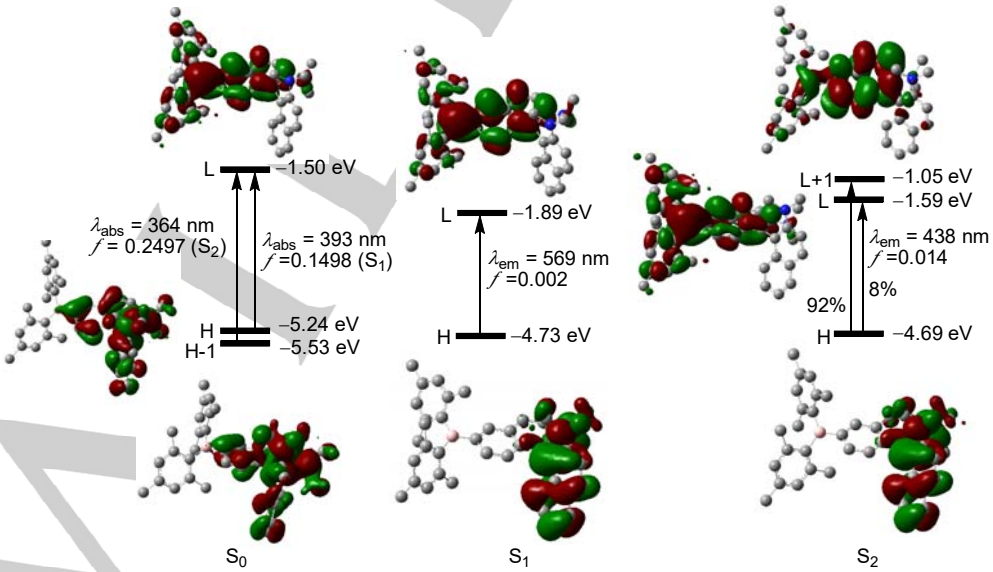

Figure 4. The Kohn-Sham energy levels, frontier orbitals, and transitions of **MBNMe$_2$-BNaph** in the ground state and the excited states, calculated at TD/PBE0/6-31G(d).

connected through a single bond is very important for the highly sensitive temperature-dependent dual fluorescence property.

Photophysical properties of CHONMe$_2$-BNaph and CNNMe$_2$-BNaph

Encouraged by the superiority of **BNMe$_2$-BNaph** over **MBNMe$_2$-BNaph** in performance as the ratiometric fluorescence thermometer, we were very interested in the general utility of this molecular design. Herein, the photophysical properties of **CHONMe$_2$-BNaph** and **CNNMe$_2$-BNaph**, which are also characteristic of the structure consisting of two D-π-A subunits connected through a single bond, were fully characterized experimentally and theoretically. In these two compounds, the electron-accepting Mes$_2$B groups are replaced by the more general electron-acceptors, CHO and CN, respectively.

The absorption and emission spectra at room temperature are shown in Figure 5. The replacement of Mes$_2$B by CHO and CN causes a blue shift of ca. 20 nm and a significant decrease of intensity for the longest absorption maxima. More interestingly, these two 1,1'-binaphthyls are also dual fluorescent. Compared with **BNMe$_2$-BNaph**, the longer wavelength band of **CHONMe$_2$-BNaph** is located at the almost the same position ($\Delta\lambda$ = 4 nm) while the shorter wavelength band is blue shifted by 15 nm. Among these three 1,1'-binaphthyls, **CNNMe$_2$-BNaph** shows fluorescence at the most blue-shifted position. A common feature was noted between **CHONMe$_2$-BNaph** and **CNNMe$_2$-BNaph** regarding the fluorescence. The fluorescence of these two compounds is dominated by the longer wavelength band, which is in contrast to the stronger intensity of the shorter wavelength band than the longer wavelength band for **BNMe$_2$-BNaph**. Based on the absorption and emission spectra in various solvents, it is easy to see that the longer emission bands of **CHONMe$_2$-BNaph** and **CNNMe$_2$-BNaph** exhibit remarkably positive solvatochromism (Figure 6). From cyclohexane and MeCN, 104 nm shift from 446 nm to 550 nm and 74 nm shift from 442 nm and 516 nm were observed for **CHONMe$_2$-BNaph** and **CNNMe$_2$-BNaph**, respectively. In contrast to the large solvatochromism of longer wavelength band, the position of the shorter wavelength band is actually not affected by the solvent polarity. In THF and

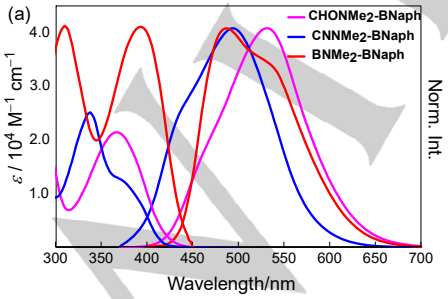

Figure 5. Absorption and fluorescence spectra of 1,1'-binaphthyls consisting of two D-π-A subunits in MOE,.

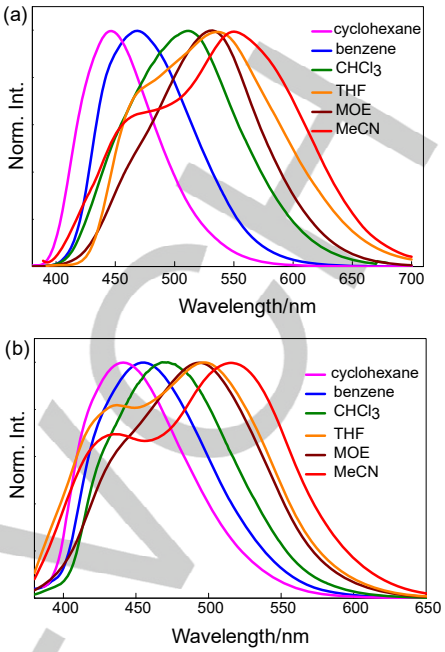

Figure 6. Fluorescence spectra of (a) **CHOBNMe$_2$-BNaph**, and (b) **CNBNMe$_2$-BNaphi** n various solvents.

MeCN, in which the shorter wavelength bands are easily detected, the shorter wavelength bands are located at the same positions for **CHONMe$_2$-BNaph** and **CNNMe$_2$-BNaph** (471 nm for **CHONMe$_2$-BNaph** and 437 nm for **CNNMe$_2$-BNaph**).

Most interestingly, the fluorescence is sensitive to temperature for both **CHONMe$_2$-BNaph** and **CNNMe$_2$-BNaph** (Figure 7 and Figure 8). In addition, the fluorescence changes in a similar manner as **BNMe$_2$-BNaph**. Namely, the intensity ratio between the shorter and longer wavelength bands increases with the increasing temperature, together with the great enhancement of fluorescence. Moreover, the linear relationships between the fluorescence intensity ratio and temperature were observed within certain temperature ranges, which are from 10 to 80 °C and from –20 to 60 °C for **CHONMe$_2$-BNaph** and **CNNMe$_2$-BNaph**, respectively. Within these temperature ranges, the CIE coordinates also changed linearly. Accompanying the significant fluorescence spectra changes, the fluorescence colour changed remarkably from yellowish green to bluish green, and green to blue for **CHONMe$_2$-BNaph** and **CNNMe$_2$-BNaph**, respectively. Furthermore, the thermochromic responses of both compounds are reversible (Figure S6). The temperature-dependence dual fluorescence behaviours of **CHONMe$_2$-BNaph** and **CNNMe$_2$-BNaph** clear suggest their great application potentials as the ratiometric fluorescence thermometers. Although the fluorescence changes in a similar trend, there still exist two different features between the three 1,1'-binaphthyl derivatives owing to the influence of different electron- acceptors. It was first noted that the separation degree of two emission bands is different. The two emission bands of **CHONMe$_2$-BNaph** are most separated. For example, the $\Delta\lambda$s of two emission bands are 119,

10.1002/chem.201901719

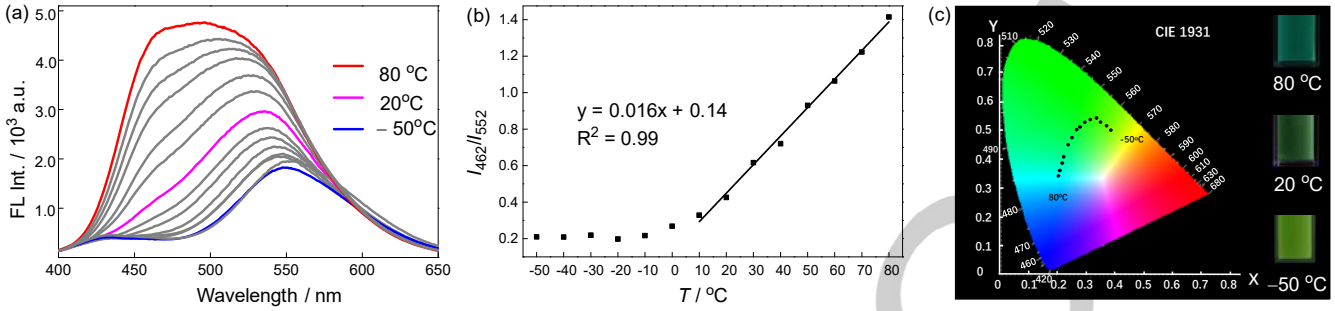

Figure 7. (a) Fluorescence spectra, (b) fluorescence intensity ratios between shorter and longer wavelength bands, and (c) photographs of the fluorescence and a diagram showing CIE coordinated (CIE 1931) at various temperatures for **CHOBNMe$_2$-BNaph** (1.0×10^{-5} M in MOE).

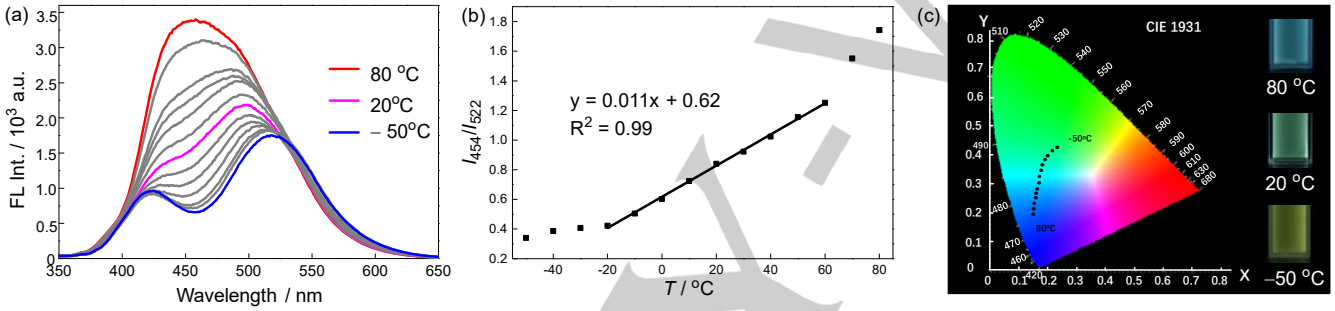

Figure 8. (a) Fluorescence spectra, (b) fluorescence intensity ratios between shorter and longer wavelength bands, (c) photographs of the fluorescence and a diagram showing CIE coordinated (CIE 1931) at various temperatures for **CNBNMe$_2$-BNaph** (1.0×10^{-5} M in MOE).

90 and 87 nm at –50 °C for **CHONMe$_2$-BNaph**, **CNNMe$_2$-BNaph** and **BNMe$_2$-BNaph**, corresponding to the $\Delta\nu$s of 5060, 4110 and 3220 cm^{-1}, respectively. Another different feature is reflected in the sensitivity of the fluorescence intensity ratio versus temperature. The Mes$_2$B-substituted compound **BNMe$_2$-BNaph** is most sensitive while the sensitivity of other two compounds is very similar with smaller slopes of 0.016 for **CHONMe$_2$-BNaph** and 0.013 for **CNNMe$_2$-BNaph**, respectively. In spite of these differences, these experimental results clear suggest that the 1,1'-binaphthyl, which consists of two D-π-A subunits, can be used as a general skeleton to achieve the temperature-dependent dual fluorescence. The temperature-dependent dual fluorescence behaviours, such as relative intensity of two emission bands, the separation of two emissions bands and the sensitivity of fluorescence intensity ratio versus temperature, are greatly influence by the electron-acceptors.

To further clarify the effect of electron-acceptor on the temperature-dependent dual fluorescence behaviours, comprehensive theoretical calculations were also performed for **CHONMe$_2$-BNaph** and **CNNMe$_2$-BNaph** (Figure 8). In S_0 state, the HOMO of both compound can spread over the entire 2,2'-diamino-1,1'-binaphthyl skeleton, which is very similar to the HOMO of **BNMe$_2$-BNaph**. In contrast to the localization of LUMO and LUMO+1 on each subunit in **BNMe$_2$-BNaph**, the LUMO and LUMO+1 in **CHONMe$_2$-BNaph**and **CNNMe$_2$-BNaph** are still delocalized over the entire 1,1'-binaphthyl framework with great contribution from electron-acceptors. Despite the different electron distribution of unoccupied frontier orbitals of **CHONMe$_2$-BNaph** and **CNNMe$_2$-BNaph** compared with **BNMe$_2$-BNaph**, the LUMO and LUMO+1 are also degenerated for **CHONMe$_2$-BNaph** and **CNNMe$_2$-BNaph**. As the result of degeneration of LUMO and LUMO+1, the excitations to S_1 and S_2 states, which are essentially assigned to HOMO→LUMO and HOMO→LUMO+1 transitions show very small differences in energy (ΔE = 0.10 eV **CHONMe$_2$-BNaph**, and 0.11 for **CNNMe$_2$-BNaph**). The very close energy of S_1 and S_2 at the Frank-Condon geometry is an important feature that enables the thermal equilibrium between them. Notably, the oscillator strength of S_1 state is about 4 times of that of S_2 state for **CHONMe$_2$-BNaph** and 10 times for **CNNMe$_2$-BNaph**, which is in contrast to the similar oscillator strengths between S_1 and S_2 for **BNMe$_2$-BNaph**. The smaller oscillator strength of S_2 state than S_1 state in **CHONMe$_2$-BNaph** and **CNNMe$_2$-BNaph** suggests its lower transition probability, which is probably partially accounts for the relative lower intensity of shorter wavelength band than longer wavelength band in **CHONMe$_2$-BNaph** and **CNNMe$_2$-BNaph**. Regarding the excited states, it was noted that the S_1 deactivations are both ascribed to the inter-subunit charge transfer from dimethylaminonaphthyl of one subunit to the naphthyl with contribution from acceptor of another subunit with small oscillator strengths (f = 0.002 for **CHONMe$_2$-BNaph**, 0.0033 for **CNNMe$_2$-BNaph**). Therefore, the S_1 states exhibit similar electronic features for all the 1,1'-

10.1002/chem.201901719

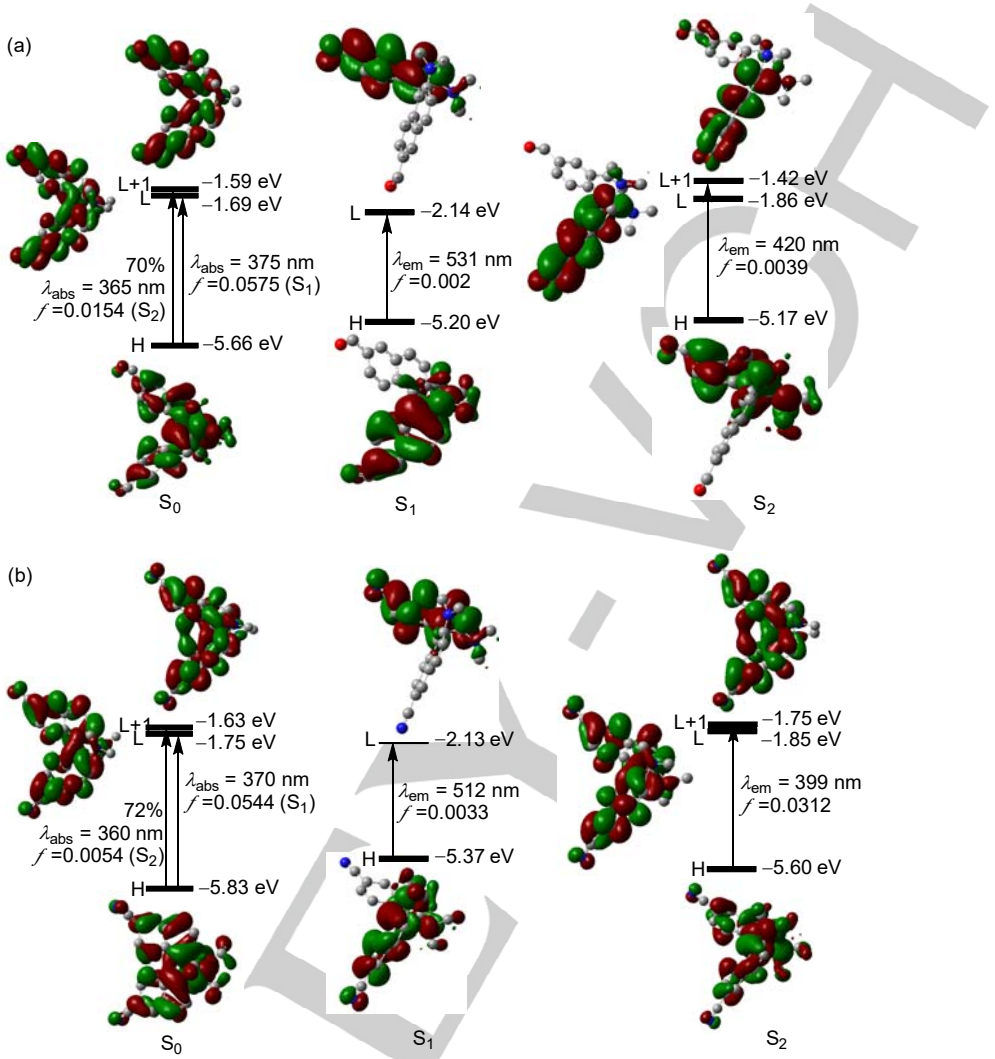

Figure 8. The Kohn-Sham energy levels, frontier orbitals, and transitions of (a) **CHONMe$_2$-BNaph** and **CNNMe$_2$-BNaph** in the ground state and the excited states, calculated at TD/PBE0/6-31G(d).

binaphthys consisting of two D-π-A subunits. However, the different electronic features were found in the S_2 states. The S_2 state deactivation of **CHONMe$_2$- BNaph** mainly consists of a HOMO→LUMO+1 transition, in which the HOMO is located on the dimethylaminonathphyl of one subunit while the LUMO spreads over the formylnaphthtyl of another subunit with intermediate contribution from formyl group of the same subunit. For **CNNMe$_2$-BNaph**, the electronic distribution of frontier orbitals in S_2 is very similar to that in S_0 state. The deactivation of S_2 is ascribed to the transition from HOMO delocalized over entire 2,2'-diamino-1,1'-binaphthyl skeleton to the LUMO+1 spreading over 6,6'-dicyano-1,1'-binaphthyl moiety. In addition to the different electronic distributions of the involved frontier orbitals, it was noted that the oscillator strength is less contrast between S_1 and S_2 deactivations for **CHONMe$_2$-BNaph** and **CNNMe$_2$-BNaph** than **BNMe$_2$-BNaph**. The oscillator strength of S_2 deactivation is only about two times of that of S_1 deactivation for **CHONMe$_2$-BNaph** and 10 times for **CNNMe$_2$-BNaph**. This is probably partially related to their less sensitivity of the fluorescence intensity ratio versus temperature. Although the accuracy of the calculated photophysical property data is not sufficiently high by this level of calculation, these calculation results definitely support that the structure feature of 1,1'-binaphthyls symmetrically consisting of two D-π-A subunits can ensure a small energy gap between S_1 and S_2 states at the Frank-Condon geometry, which enables the thermal equilibrium between them. In addition, the emission of two bands are greatly affected by the electron-acceptors.

Conclusions

In summary, we herein have explored the importance of the structure feature of **BNMe$_2$-BNaph** and the general utility of this molecular design for the temperature-dependent dual fluorescence. A detailed comparison of the photophysical properties between **BNMe$_2$-BNaph** and the reference compound **MBNMe$_2$-BNaph**, which lacks one electron-accepting Mes_2B, suggest that the structure of **BNMe$_2$-BNaph** symmetrically consisting of two D-π-A subunits is important to achieve highly sensitive temperature-dependent dual fluorescence. In line with this molecular design, it was found another two 1,1'-binaphthyls consisting of two D-π-A subunits, in which Mes_2B groups were replaced by CHO and CN, respectively, also show temperature-dependent dual fluorescence with similar change trend, denoting the great potential applications of these compounds as ratiometric fluorescence thermometers and the general utility of the current molecular design for temperature-dependent dual fluorescence. The temperature-dependent dual fluorescence behaviors, such as relative intensity of two emission bands, the separation of two emissions bands and the sensitivity of fluorescence intensity ratio versus temperature, are greatly influence by the electron-acceptors. Dual fluorescence with anti-kasha's rule is already an anomalous photophysical phenomenon for SOMs. The achievement of temperature-dependent dual fluorescence is even much more challenging. Our molecular design can provide a general method to achieve this fascinating property. Considering the promising application of temperature-dependent dual fluorescence of SOMs in ratiometric fluorescence measurement of temperature, the current results will definitely provide ground basis for the further new molecular designs to obtain SOMs-based ratiometric fluorescence thermometers with more optimized performance for various applications.

Experimental Section

General

Melting points (M.p.) were measured on a Tektronix XT-4 instrument. ^{1}H and ^{13}C NMR spectra were recorded with a Bruker 400 spectrometer. High resolution mass spectra (HRMS) were obtained using an electrospray ionization time-of-flight 4(ESI-TOF) mass spectrometer. UV-vis absorption spectra and fluorescence spectra measurements were performed with a Hitachi U-2910 spectrometer and a Hitachi F-7000 spectrometer, respectively. All reactions were carried out under nitrogen atmosphere. The starting material 6,6'-dibromo-2,2'-bis (N,N-dimethylamino)-1,1'-binaphthyl (**BrNMe$_2$-BNaph**) was prepared according to the literature.[12]

Synthesis

6-Dimesitylboryl-2,2'-bis(N,N-dimethylamino)-1,1'-binaphthyl (MBNMe$_2$-BNaph): To a solution of **BrNMe$_2$-BNaph** (1.25 g, 2.5 mmol) in anhydrous THF (50 ml) was added a hexane solution of *n*-BuLi (1.72 ml, 1.6 M, 2.75 mmol) dropwise via a syringe at –78 ℃ under a stream of nitrogen. The mixture was stirred at the same temperature for 1 h. MeOH was added to quenching the reaction via syringe. After the mixture was warmed to room temperature, the aqueous layer was extracted with CH_2Cl_2. The combined organic layer was dried over anhydrous Na_2SO_4, filtered and concentrated under reduced pressure. To a solution of the resulting mixture in anhydrous THF (50 ml) was added a hexane solution of *n*-BuLi (1.72 ml, 1.6 M, 2.75 mmol) dropwise via a syringe at –78 ºC under a stream of nitrogen, and stirred at the same temperature for 1 h. A solution of dimesitylfluoroborane (1 g, 3.75 mmol) in anhydrous THF (15 ml) was added to the reaction mixture via syringe. The reaction mixture was warmed to room temperature slowly and stirred overnight. The reaction mixture was concentrated under reduced pressure. The resulting mixture was subjected to a silica gel chromatography (5/1 petroleum ether/ethyl acetate, R_f = 0.40) to afford 0.69 g (1.17 mmol) of **MBNMe$_2$-BNaph** in 47% yield as greenish yellow solids. M.p. 248.5-250.5 ºC; ^{1}H NMR ($CDCl_3$, 400 MHz): δ 8.01 (s, 1H), 7.84 (d, *J* = 5.5 Hz, 2H), 7.79 (d, *J* = 7.8 Hz, 1H), 7.44 (d, *J* = 8.7 Hz, 1H), 7.37 (d, *J* = 8.8 Hz, 1H), 7.29 (d, *J* = 6.5 Hz, 1H), 7.24 (d, *J* = 9.3 Hz, 2H), 7.18 (d, *J* = 8.0 Hz, 1H), 7.00 (d, *J* = 8.6 Hz, 1H), 6.80 (s, 4H), 2.50 (s, 6H), 2.45 (s, 6H), 2.30 (s, 6H), 2.00 (s, 12H); ^{13}C NMR ($CDCl_3$, 100 MHz): δ 142.0, 140.8, 138.7, 138.2, 134.6, 132.8, 130.3, 128.6, 128.1, 127.8, 126.2, 125.9, 124.9, 123.5, 120.6, 119.8, 43.4, 42.9, 23.4, 21.2; HRMS (ESI-TOF): 589.3750 $[M+H]^+$ Calcd for $C_{42}H_{46}{}^{11}BN_2$: 589.3749.

6,6'-Diformyl-2,2'-bis(N,N-dimethylamino)-1,1'-binaphthyl (CHONMe$_2$-BNaph): To a solution of $BrNMe_2$-BNaph (0.85 mg, 2.1 mmol) in anhydrous THF (80 ml) was added a hexane solution of *n*-BuLi (2.88 ml, 1.6 M, 4.6 mmol) dropwise via a syringe at –78 ºC under a stream of nitrogen. The mixture was stirred at the same temperature for 2 h. Anhydrous DMF (5 ml) was added to the reaction mixture via syringe. The reaction mixture was warmed to room temperature slowly and stirred overnight. The reaction mixture was concentrated under reduced pressure. The resulting mixture was subjected to a silica gel chromatography (5/2 petroleum ether/ethyl acetate, R_f = 0.45) to afford 297 mg (0.75 mmol) of **CHONMe$_2$-BNaph** in 36% yield as yellow solids. M.p. 294-295 ºC; ^{1}H NMR ($CDCl_3$, 400 MHz): δ10.06 (s, 2H), 8.28 (s, 2H), 8.00 (d, *J* = 8,9 Hz, 2H), 7.64 (dd, *J* = 8.9, 1.6 Hz, 2H), 7.46 (d, *J* = 8.7 Hz, 2H), 7.21 (d, *J* = 8.9 Hz, 2H), 2.55 (s, 12H); ^{13}C NMR ($CDCl_3$, 100 MHz): δ 190.8, 151.1, 137.2, 133.6, 130.5, 129.6, 126.6, 125.1, 122.6, 121.2, 119.8, 41.4; HRMS (ESI-TOF): 397.1914 $[M+H]^+$ Calcd for $C_{26}H_{25}N_2O_2$: 397.1911.

6,6'-Dicyano-2,2'-bis(N,N'-diphenylamino)-1,1'-binaphthyl (CNNMe$_2$-BNaph): An Schlenk tube was charged with **BrNMe$_2$-BNaph** (1.0 g, 2.0 mmol), CuCN (447.8mg, 5 mmol) and degassed anhydrous DMF (30 ml). The mixture was stirred overnight at 150 ℃. After the mixture was cooled to room temperature, a saturated solution of NaOH was added, and the aqueous layer was extracted with CH_2Cl_2. The combined organic layer was dried over anhydrous Na_2SO_4, filtered and concentrated under reduced pressure. The purification by a silica gel chromatography (3/1 petroleum ether/ethyl acetate, R_f = 0.35) afforded 350 mg (0.9 mmol) of **CNNMe$_2$-BNaph** in 45% yield as deep yellow solids. M.p. > 300 ºC; ^{1}H NMR (400 MHz, $CDCl_3$): δ

8.16 (s, 2H), 7.89 (d, *J* = 8.9 Hz, 2H), 7.49 (s, 2H), 7.30 (dd, *J* = 8.9, 1.6 Hz, 2H), 7.12 (d, *J* = 8.9 Hz, 2H), 2.55 (s, 12H); ^{13}C NMR ($CDCl_3$, 100 MHz): δ 151.6, 136.2, 134.2, 129.7, 127.6, 127.2, 126.1, 121.4, 119.7, 42.5; HRMS (DART Positive): 391.1922 $[M+H]^+$ Calcd for $C_{26}H_{23}N_4$: 391.1917.

Computational methods

All calculations were conducted by using the Gaussian 09 program.[15] The PBE0/6-31G(d) level of theory was used for all the calculations. To ensure that the optimized geometry was at a minimum, all geometry optimizations were followed by a frequency calculation and only positive frequencies were obtained. Based on the optimized ground state structure, the vertical transitions and optimized geometries of the first two excited states were calculated and by TD-DFT method.

Acknowledgements

The National Natural Science Foundation of China (Grants 21572120, 21473214) and the Strategic Priority Research Program of the Chinese Academy of Science (XDB12020200) are greatly acknowledged for financial support. The HPC Cloud Platform of Shandong University is sincerely acknowledged for the support in the theoretical calculations.

Keywords: temperature-dependent dual fluorescence • D-π-A • intramolecular charge transfer • 1,1'-binaphthyl • anti-kasha's rule

[1] a) X.-D. Wang, O. S. Wolfbeis, R. J. Meier, *Chem. Soc. Rev*. **2013**, *42*, 7834–7869; b) E. J. McLaurin, L. R. Bradshaw, D. R. Gamelin, *Chem. Mater*. **2013**, *25*, 1283–1292; c) Y. Cui, F. Zhu, B. Chen, G. Qian, *Chem. Commun*. **2015**, *51*, 7420-7431.

[2] a) Y. Wu, J. Liu, J. Ma, Y. Lin, Y. Wang, D. Wu, *ACS Appl. Mater. Interfaces*. **2016**, *8*, 14396–14405; b) A. E. Albers, E. M. Chan, P. M. McBride, C. M. Ajo-Franklin, B. E. Cohen, B. A. Helms, *J. Am. Chem. Soc.* **2012**, *134*, 9565–9568; c) X. Cui, Y. Cheng, H. Lin, F. Huang, Q. Wu, Y. Wang, *Nanoscale.* **2017**, *9*, 13794-13799; d) E. J. McLaurin, L .R. Bradshaw, D. R. Gamelin, *Chem. Mater.* **2013**, *25*, 1283–1292.

[3] a) J. Qiao, Y.-H. Wang, C.-F. Chen, L. Qi, P. Dong, X.-Y. Mu, D.-P. Kim, *Anal. Chem.* **2015**, *87*, 10535–10541; b) F. Ye, C. Wu, Y. Jin, Y.-H. Chan, X. Zhang, D. T. Chiu, *J. Am. Chem. Soc.* **2011**, *133*, 8146–8149; c) H. Zhang, J. Jiang, P. Gao, T. Yang, K. Y. Zhang, Z. Chen, S. Liu, W. Huang, Q. Zhao, *ACS. Appl. Mater. Interfaces.* **2018**, *10*, 17542−17550.

[4] a) Y. Cui, R. Song, J. Yu, M. Liu, Z. Wang, C. Wu, Y. Yang, Z. Wang, B. Chen, G. Qian, *Adv. Mater.* **2015**, *27*, 1420-1425; b) X. Rao, T. Song, J. Gao, Y. Cui, Y. Yang, C. Wu, B. Che, G. Qian, *J. Am. Chem. Soc.* **2013**, *135*, 15559-15564.

[5] a) C. Cao, X. Liu, Q. Qiao, M. Zhao, W. Yin, D. Mao, H. Zhang, Z. Xu, *Chem. Commun.* **2014**, *50*, 15811–15814; b) Q. Zhu, W. Yang, S. Zheng, H. H. Y. Sung, I. D. Williams, S. Liu, B. Z. Tang, *J. Mater. Chem. C*. **2016**, *4*, 7383–7386; c) Q. Fang, J. Li, S. Li, R. Duan, S. Wang, Y. Yi, X. Guo, Y. Qian, W. Huang, G. Yang, *Chem. Commun.* **2017**, *53*, 5702–5705; d) N. Chandrasekharan, L. A. Kelly, *J. Am. Chem. Soc.* **2001**, *123*, 9898–9899; e) L. Shi, W. Song, C. Lian, W. Chen, J. Mei, J. Su, H. Li, H. Tian, *Adv. Optical. Mater.* **2018**, *6*, 1800190; f) B. Sk, S. Khodia, A.Patra, *Chem. Commun.* **2018**, *54*, 1786–1789; g) J. Feng, K. Tian, D. Hu, S. Wang, S. Li, Y. Zeng, Y. Li, G. Yang, *Angew. Chem*. **2011**, *123*, 8222 – 8226; *Angew. Chem. Int. Ed.* **2011**, *50*, 8072–8076; h) B. Sk, S. Khodia, A. Patra, *Chem. Commun.* **2018**, *54*, 1786–1789.

[6] M. Kasha, Discussions of the Faraday Society, **1950**, *9*, 14.

[7] a) C. Yuan, S. Saito, C. Camacho, S. Irle, I. Hisaki, S. Yamaguchi, *J. Am. Chem. Soc*. **2013**, *135*, 8842–8845; b) C. Yuan, S. Saito, C. Camacho, T. Kowalczyk, S. Irle, S. Yamaguchi, *Chem. Eur. J.* **2014**, *20*, 2193–2200.

[8] a) Z. Zhang, Y.-S. Wu, K.-C. Tang, C.-L. Chen, J.-W. Ho, J. Su, H. Tian, P.-T. Chou, *J. Am. Chem. Soc*. **2015**, *137*, 8509–8520; b) W. Chen, C.-L. Chen, Z. Zhang, Y.-A. Chen, W.-C. Chao, J. Su, H. Tian, P.-T. Chou, *J. Am. Chem. Soc*. **2017**, *139*, 1636–1644; c) Z. Zhang, C.-L. Chen, Y.-A. Chen, Y.-C. Wei, J. Su, H. Tian, P.-T. Chou, *Angew. Chem*. **2018**, *130*, 10028 –10032; *Angew. Chem. Int. Ed*. **2018**, *57*, 9880–9884.

[9] a) E. Lippert, W. Lüder, F. Moll, W. Nägele, H. Boos, H. Prigge, I. Seibold-Blankenstein, *Angew. Chem.* **1961**, *73*, 695-706; b) H. Naito, K. Nishino, Y. Morisaki, K. Tanaka, Y. Chujo, *Angew. Chem*. **2017**, *129*, 260 –265; *Angew. Chem. Int. Ed.* **2017**, *56*, 254–259; c) A. Ito, S. Ishizaka, N. Kitamura, *Phys. Chem. Chem. Phys*. **2010**, *12*, 6641–6649; d) A. Köhn, C. Hättig, *J. Am. Chem. Soc.* **2004**, *126*, 7399-7410; e) S. D. Choudhury, S. Muralidharan, H. Pal, *Phys. Chem. Chem. Phys*. **2014**, *16*, 11509–11518.

[10] a) A. P. Demchenko, V. I. Tomin, P.-T. Chou, *Chem. Rev*. **2017**, *117*, 13353–13381; b) T. Itoh, *Chem. Rev*. **2012**, *112*, 4541–4568.

[11] a) H. Pan, G.-L. Fu, Y.-H. Zhao, C.-H. Zhao, *Org. Lett*. **2011**, *13*, 4830–4833; b) C. Wang, J. Jia, W.-N. Zhang, H.-Y. Zhang, C.-H. Zhao, *Chem. Eur. J*. **2014**, *20*, 16590–16601; c) C. Wang, Q.-W. Xu, W.-N. Zhang, Q. Peng, C.-H. Zhao, *J. Org. Chem*. **2015**, *80*, 10914–10924; d) C. Wang, Z.-B. Sun, Q.-W. Xu, C.-H. Zhao, *Chem. Eur. J.* **2016**, *22*, 16750–16754; e) S.-Y. Li, Y.-J. Hui, Z.-B. Sun, C.-H. Zhao, *Chem. Commun*. **2017**, *53*, 3446–3449; f) M.-Y. Zhang, Z.-Y. Li, B. Lu, Y. Wang, Y.-D. Ma, C.-H. Zhao, *Org. Lett*. **2018**, *20*, 6868–6871; g) Z.-H. Zhao, M.-Y. Zhang, D.-H. Liu, C. H. Zhao, *Org. Lett.* **2018**, *20*, 7590–7593.

[12] Z.-B. Sun, J.-K. Liu, D.-F. Yuan, Z.-H. Zhao, X.-Z. Zhu, D.-H. Liu, Q. Peng, C.-H. Zhao, *Angew. Chem.* **2019**, *131*, 4894 –4900; *Angew. Chem. Int. Ed.* **2019**, *58*, 4840-4846.

[13] a) L. Ji, S. Griesbeck, T. B. Marder, *Chem. Sci.* **2017**, *8*, 846–863; b) A. Wakamiya, S. Yamaguchi, *Bull. Chem. Soc. Jpn*. **2015**, *88*, 1357–1377; c) Y. Ren, F. Jäkle, *Dalton Trans*. **2016**, *45*, 13996–14007; d) Z. M. Hudson, S. Wang, *Acc. Chem. Soc.* **2009**, *42*, 1584–1596; e) Z.-B. Sun, S.-Y. Li, Z.-Q. Liu, C.-H. Zhao, *Chin. Chem. Lett.* **2016**, *27*, 1131–1138; f) S.-Y. Li, Z.-B. Sun, C.-H. Zhao, *Inorg. Chem.* **2017**, *56*, 8705–8717; g) C. D. Entwistle, T. B. Marder, *Angew. Chem*. **2002**, *114*, 3051 –3056; *Angew. Chem. Int. Ed*. **2002**, *41*, 2927–2931.

[14] H. W. Lee, M. K. Cho, H.-R. Kim, C. S. Lim, C. Kang, H. M. Kim, *Chem. Commun*. **2017**, *53*, 6097–6100.

[15] M. J. Frisch, G. W. Trucks, H. B. Schlegel, G. E. Scuseria, M. A. Robb, J. R. Cheeseman, G. Scalmani, V. Barone, B. Mennucci, G. A. Petersson, H. Nakatsuji, M. Caricato, X. Li, H. P. Hratchian, A. F. Izmaylov, J. Bloino, G. Zheng, J. L. Sonnenberg, M. Hada, M. Ehara, K. Toyota, R. Fukuda, J. Hasegawa, M. Ishida, T. Nakajima, Y. Honda, O. Kitao, H. Nakai, T. Vreven, J. A. Montgomery, Jr., J. E. Peralta, F. Ogliaro, M. Bearpark, J. J. Heyd, E. Brothers, K. N. Kudin, V. N. Staroverov, T. Keith, R. Kobayashi, J. Normand, K. Raghavachari, A. Rendell, J. C. Burant, S. S. Iyengar, J. Tomasi, M. Cossi, N. Rega, J. M. Millam, M. Klene, J. E. Knox, J. B. Cross, V. Bakken, C. Adamo, J. Jaramillo, R. Gomperts, R. E. Stratmann, O. Yazyev, A. J. Austin, R. Cammi, C. Pomelli, J. W. Ochterski, R. L. Martin, K. Morokuma, V. G. Zakrzewski, G. A. Voth, P. Salvador, J. J. Dannenberg, S. Dapprich, A. D. Daniels, O. Farkas, J. B. Foresman, J. V. Ortiz, J. Cioslowski, and D. J. Fox, Gaussian 09, Revision B.01, Gaussian, Inc., Wallingford CT, 2010.

10.1002/chem.201901719

WILEY-VCH

Entry for the Table of Contents

FULL PAPER

All the 1,1'-binaphthyls, which are characteristic of the composition of two D-π-A subunits with two dimethylamino groups and two electron-acceptors (dimesitylboryl, formyl and cyano) at 2,2'- and 6,6'-positions, respectively, display temperature-dependent dual fluorescence property.

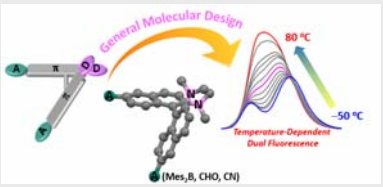

Di-Hong Liu, Zuo-Bang Sun, Zheng-Hua Zhao, Qian Peng, Cui-Hua Zhao**

Page No. – Page No.

1'-Binaphthyl Consisting of Two Donor-π-acceptor Subunits : a General Skeleton for Temperature-Dependent Dual Fluorescence